The 2010 IEEE/RSJ International Conference on
Intelligent Robots and Systems
October 18-22, 2010, Taipei, Taiwan

Virtual Mass of Impedance System for Free-Flying Target Capture

Hiroki Nakanishi, Naohiro Uyama, and Kazuya Yoshida,

Abstract— **This paper discusses the target motion around the contact in the satellite capture operation using a free-flying space robot. The contact force has the potential for pushing the target beyond the manipulator reach or making the target have a tumbling motion. An impedance control is useful to prevent the robot hand from pushing the target. However, the relationship between the dynamics parameters, contact characteristics, and target motion have not been clarified yet. In this paper, virtual mass of impedance system (VMI) model is proposed to represent the influence of the hand impedance on the target motion. Using this model, the condition to prevent the robot pushing the target away is clarified.**

I. Introduction

With the increasing number of satellites in orbit, service and rescue missions are also becoming more important. In the case of non-contingent services on operational satellites, refueling is beneficial for extending the mission life and replacements of on-board components are effective for ensuring that the platforms will continue in the future. In the case of contingent servicing or rescue, re-orbiting stranded and end-of-life satellites will become the primary focus. If such malfunctioning satellites drift in orbit, they become potential hazards to other operational satellites. In 2009, Illidium, a commercial satellite owned by a U.S. company was destroyed in a collision with a defunct Russian military satellite Cosmos 2251. This collision alone caused more than 500 new debris.

In order to perform such service and rescue missions, dedicated robotic technology is required. The Engineering Test Satellite VII (ETS-VII) was launched by NASDA, Japan, in 1997-1999 to establish a solid basis for the technology of autonomous rendezvous-docking and robotic operations on an unmanned satellite [1]. Orbital Express, which was launched in 2007 by DARPA, successfully demonstrated autonomous rendezvous-docking and refueling service [2]. However, those demonstrations were limited to operations with a cooperative target. Here, "cooperative" implies the existence of attitude stabilization, signal-responding devices (transponders and/or optical markers), and dedicated fixtures on the target. However, in practical future service and rescue missions, most targets are non-cooperative in terms of the lack of dedicated fixtures and attitude stabilization. In this case, the gripper can potentially push the target away during the capture sequence. Therefore, the robot hand should be carefully controlled so that it can give minimum impact on the target.

The authors are with the Department of Aerospace Engineering, Graduate School of Engineering, Tohoku University, 6-6-01 Aramaki-aza-Aoba, Sendai, 980-0871, Japan {nakanisi, uyama, yoshida}@astro.mech.tohoku.ac.jp

Impedance control is useful to control the impact. The authors have demonstrated that an impedance control can prevent the robot hand from pushing the target [3]. Moosavian et al. proposed a method that provides impedance characteristics for the manipulator, the grasped object, and the base of a free-flying robot. [4]. Pathak et al. also proposed an impedance control method [5]. However, the relationship between the impedance characteristics, dynamics parameters, contact characteristics, and target motion have not been clarified yet.

The idea of equivalent mass is useful criteria to express the contact motion; these provide motion variations in the contact phenomena employing simple formulae. Asada proposed the idea of the generalized inertia ellipsoid (GIE)[6]. The GIE introduces the concept of virtual inertia for a free-joint link system, wherein the inertias of all links are projected onto the hand position of the manipulator. Yoshida et al. proposed the extended inversed inertia tensor, which is an extension of the GIE. Their inertia tensor includes the effect of joint damping and stiffness using a virtual rotor [7]. However, the relationship between the virtual rotor and the viscosity or stiffness is not clarified.

In this paper, in other to evaluate the relationship, "virtual mass of impedance system (VMI)" model is redefined to represent the influence of the hand impedance on the target motion. This model is an extension of the equivalent mass concepts so that it can be applied to a multi-body impedance system. By using the concept, the appropriate impedance condition to prevent the pushing of the target away after the initial contact is discussed.

II. Dynamics and Control of Satellite Capture

A. Assumption

In this chapter, a free-flying space robot (hereinafter called "chaser") is assumed to consist of a rigid main body and an n DOF serial link manipulator. The target satellite is also a rigid body. The chaser has already completed the rendezvous with the target. In other to capture the target, the chaser's manipulator makes contact with the target surface. Figure 1 shows the image of the system of satellite capture.

B. Chaser Model

The dynamic equations of a free-flying robot with a manipulator arm are given as follows:

$$\begin{bmatrix} \mathcal{F}_b \\ \boldsymbol{\tau} \end{bmatrix} = \begin{bmatrix} \boldsymbol{H}_b & \boldsymbol{H}_{bm} \\ \boldsymbol{H}_{bm}^T & \boldsymbol{H}_m \end{bmatrix} \begin{bmatrix} \ddot{\boldsymbol{x}}_b \\ \ddot{\boldsymbol{\phi}} \end{bmatrix} + \begin{bmatrix} \boldsymbol{c}_b \\ \boldsymbol{c}_m \end{bmatrix} - \begin{bmatrix} \boldsymbol{J}_b^T \\ \boldsymbol{J}_m^T \end{bmatrix} \mathcal{F}_h, \quad (1)$$

where

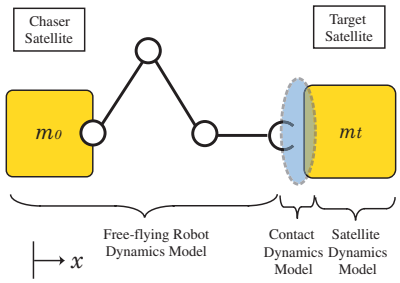

Fig. 1. Dynamics model of satellite capture

$\boldsymbol{H}_b \in R^{6\times 6}$: inertia matrix of the base
$\boldsymbol{H}_m \in R^{n\times n}$: inertia matrix of the manipulator
$\boldsymbol{H}_{bm} \in R^{6\times n}$: coupling inertia matrix between the base and manipulator
$\boldsymbol{c}_b \in R^6$: non-linear velocity dependent term of the base
$\boldsymbol{c}_m \in R^6$: non-linear velocity dependent term of the manipulator
$\boldsymbol{J}_b \in R^{6\times n}$: Jacobian matrix between the base and end tip of manipulator
$\boldsymbol{J}_m \in R^{6\times n}$: Jacobian matrix between the joints and end tip of manipulator
$\mathcal{F}_b \in R^6$: external force and moment on the gravity center of the base
$\mathcal{F}_h \in R^6$: external force and moment on the end tip of the manipulator
$\boldsymbol{\tau} \in R^n$: joint torque of the manipulator
$\boldsymbol{x}_b \in R^6$: position of the base
$\boldsymbol{\phi} \in R^n$: joint angles of the manipulator

C. Contact Model

The general form of the contact force can be formulated as follows [8]:

$$F = d\delta^p \dot{\delta}^q + k\delta^n, \tag{2}$$

where δ is the penetration. The Five parameters (d, k, p, q, and n) determine the contact force model. Further, the parameters d and k represent the viscosity and stiffness characteristics, respectively.

If one sets $p = 0$ and $q = n = 1$, Eq.(2) becomes the following linear spring-dashpot model:

$$F = d_c\dot{\delta} + k_c\delta, \tag{3}$$

where d_c is the damping coefficient, k_c is the stiffness, and subscript "c" indicates the contact surface. The formulation in this paper adopts the linear spring-dashpot model for simplicity.

D. Impedance Control for Free-Flying Space Robot

The end effector impedance control is provided by the following equation:

$$\boldsymbol{M}_i\Delta\ddot{\boldsymbol{x}}_h + \boldsymbol{D}_i\Delta\dot{\boldsymbol{x}}_h + \boldsymbol{K}_i\Delta\boldsymbol{x}_h = \mathcal{F}_h, \tag{4}$$

where $\boldsymbol{x}_h \in R^6$ denotes the position and orientation of the end effector with respect to the inertial coordinate frame, and $\Delta\boldsymbol{x}_h$ ($\equiv \boldsymbol{x}_h - \boldsymbol{x}_{hd}$) denotes the deformation from the equilibrium point $\boldsymbol{x}_{hd}$. $\boldsymbol{M}_i \in R^{6\times 6}$, $\boldsymbol{D}_i \in R^{6\times 6}$ and $\boldsymbol{K}_i \in R^{6\times 6}$ are matrices expressing the desired impedance property in inertia, viscosity, and stiffness, respectively, measured at the end effector.

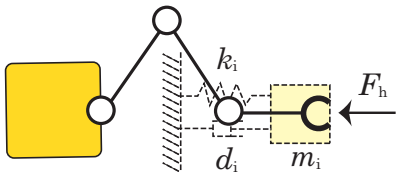

Fig. 2. Impedance control with respect to the inertial coordinate

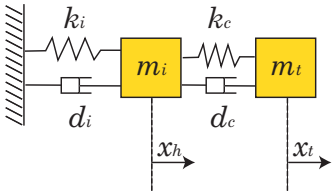

Fig. 3. 2-degree-of-freedom (DOF) system

The impedance characteristics given by Eq.(4) with respect to the inertial frame are achieved by controlling the joint velocities $\dot{\boldsymbol{\phi}}$ as follows [9]:

$$\dot{\boldsymbol{\phi}} = \boldsymbol{J}^{*-1}\left\{\int_0^t \frac{1}{\boldsymbol{M}_i}(\mathcal{F}_h - \boldsymbol{D}_i\Delta\dot{\boldsymbol{x}}_h - \boldsymbol{K}_i\Delta\boldsymbol{x}_h) + \ddot{\boldsymbol{x}}_{hd}dt - \dot{\boldsymbol{x}}_{gh}\right\}, \tag{5}$$

where $\boldsymbol{J}^* \in R^{6\times n}$ is the generalized Jacobian matrix [10], $\dot{\boldsymbol{x}}_{gh} \in R^6$ is the velocity of the gravity center of the entire system projected on the velocity of the end effector.

In general, the contact in the target capture is a three-dimensional phenomenon. However, It can be assumed as a one-dimensional phenomenon in the local viewpoint. In this case, the target mass is the GIE at the contact point [3]. Hereinafter, a one-dimensional satellite capture model is considered for simplicity. The dynamics model of a chaser robot under the impedance control is shown in Fig.2. In the figure, m_i, d_i, and k_i are mass, viscosity, and stiffness characteristics given by the control, respectively.

From another viewpoint, the contact model combines the dynamics of each object in the contact state. The entire dynamics model during the contact can be represented as a coupled-vibration system as shown in Fig.3. In this figure, x_h and x_t are the chaser hand and target position, respectively. In this case, the penetration δ in Eq.(3) is equal to $x_h - x_t$.

The equations of motion are as follows:

$$\left.\begin{aligned} m_i\ddot{x}_h + (d_i + d_c)\dot{x}_h + (k_i + k_c)x_h - d_c\dot{x}_t - k_cx_t = 0 \\ m_t\ddot{x}_t + d_c\dot{x}_t + k_cx_t - d_c\dot{x}_h - k_cx_h = 0 \end{aligned}\right\}. \tag{6}$$

Rewriting Eq.(6), a state space equation is obtained as

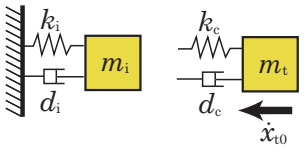

Fig. 4. Simulation model: Target collision on an impedance system

follows:

$$\frac{d}{dt}\begin{bmatrix} x_h \\ x_t \\ \dot{x}_h \\ \dot{x}_t \end{bmatrix} = \begin{bmatrix} 0 & 0 & 1 & 0 \\ 0 & 0 & 0 & 1 \\ -\frac{k_c+k_i}{m_i} & \frac{k_c}{m_i} & -\frac{d_c+d_i}{m_i} & \frac{d_c}{m_i} \\ \frac{k_i}{m_t} & -\frac{k_c}{m_t} & \frac{d_i}{m_t} & -\frac{d_c}{m_t} \end{bmatrix} \begin{bmatrix} x_h \\ x_t \\ \dot{x}_h \\ \dot{x}_t \end{bmatrix}$$

$$\frac{d}{dt}\boldsymbol{X}(t) = \boldsymbol{A}\boldsymbol{X}(t), \quad (7)$$

where $\boldsymbol{X}$ and $\boldsymbol{A}$ are the state variable and square coefficient matrix, respectively.

III. Relationship Between Manipulator Impedance and Target Post-Contact Velocity

A. Simulation Study

A contact simulation is conducted in order to investigate the relationship between the manipulator impedance and the post-contact velocity of the target. The simulation model is shown in Fig.4. In the contact, the chaser hand and target velocity is obtained by Eq.7.

Figure 5 shows the post-contact target velocity of the simulation results. The condition of the manipulator impedance is given as follows:

$$[m_i \ d_i \ k_i] = A \cdot [10 \ 300 \ 50], \quad (8)$$

where A is the magnification ratio. Hereinafter, the impedance condition that A is larger is called "higher impedance," the condition that A is smaller is called "lower impedance." The initial velocity is 0.1 [m/s]. The damping coefficient d_c and stiffness k_c of the contact surface were assumed as $d_c = 30$ [Ns/m] and $k_c = 50,000$ [N/m], respectively. The target mass was assumed as $m_t = 50$ [kg].

This result shows that the post-contact target velocity depends on the manipulator condition. In the case of higher impedance, the manipulator bounces the target. In the lower impedance case, the target pushes the manipulator. After a few collisions, the target stops. When the impedance has a medium value, the target stops after the initial contact.

B. Restitution Coefficient of Impedance

The restitution coefficient is a reasonable parameter for describing the target motion around the contact. In general, the coefficient is used in the rigid two-body contact. Here, the coefficient is redefined to include the effect of the viscosity and stiffness in the contact of the impedance system. Hereinafter, in this study, the proposed restitution coefficient is named the "restitution coefficient of impedance (RCI)" in order to differentiate from the conventional restitution coefficient. The impedance system and contact model are

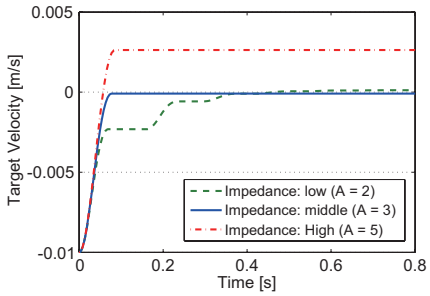

Fig. 5. Post-contact target velocity

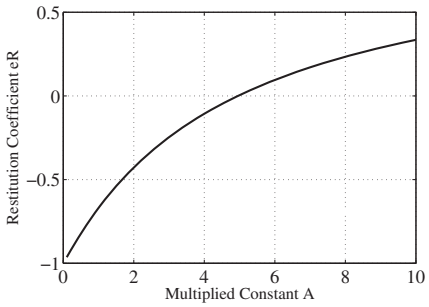

Fig. 6. Restitution coefficient e_R vs. magnification ratio A to each impedance parameter m_i, d_i, and k_i for over-damped systems ($d_i = 300$ [Ns/m])

considered as an virtual wall. The characteristics of the impedance system and contact model are projected to the RCI. The RCI reveal the manner in which the target velocity after the initial contact changes with the impedance parameters. Suppose that contact starts at time t_0 and ends at time t_e. t_e, is given as the time that the penetration $\delta = x_h - x_t$ returns to zero. The RCI e_R is defined by the relative velocity between the target's velocity $\dot{x}_t$ and the equilibrium point velocity of the hand impedance $\dot{x}_{hd}$ as follows:

$$e_R = -\frac{\dot{x}_t(t_e) - \dot{x}_{hd}(t_e)}{\dot{x}_t(t_0) - \dot{x}_{hd}(t_0)}, \quad (9)$$

The e_R is a number in the range from -1 to 1. Qualitatively, $e_R = 1$ represents that the target is bounced off with same absolute velocity as the initial one. $e_R = 0$ represents that the target stops immediately after collision. $e_R = -1$ represents that the target motion is unchanged after collision. This implies that $0 < e_R < 1$ represents that the target is bounced off by the impedance system, while $-1 < e_R < 0$ represents that the target continues toward the impedance system and repeats contact after the initial contact.

Figure 6 shows the relationship between the impedance magnitude A and RCI e_R. This result reveals that the increase of the impedance increases the e_R. The e_R has a zero value around $A = 5$. This implies that the target can be stopped by choosing the magnitude of mechanical impedance.

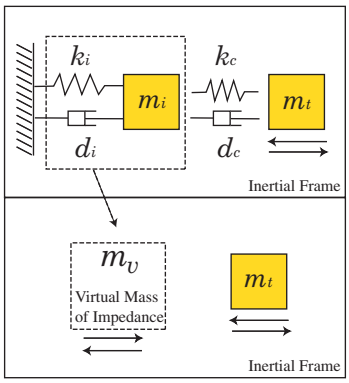

Fig. 7. Virtual mass model

IV. Virtual Mass of Impedance System

When dealing with contact phenomena of the multibody link system, the idea of virtual mass or inertia are useful to simplify the dynamics model [6][7].

The advantage of the virtual mass model is that the dynamics model becomes a simple two-body contact model in which one mass collides with another mass. The chaser's hand can be modeled as a virtual point mass having an equivalent mass value m_v. Consider the case in which the hand with an initial velocity $\dot{x}_h$ collides with a target having velocity $\dot{x}_t$. The post-collision velocities $\dot{x}'_h$ and $\dot{x}'_t$ can be calculated using the restitution coefficient e as follows:

$$\dot{x}'_h = \frac{m_v\dot{x}_h + m_t\dot{x}_t - m_t e(\dot{x}_h - \dot{x}_t)}{m_v + m_t}, \quad (10)$$

$$\dot{x}'_t = \frac{m_v\dot{x}_h + m_t\dot{x}_t + m_v e(\dot{x}_h - \dot{x}_t)}{m_v + m_t}. \quad (11)$$

Note that the e is not the RCI, e_R, but the conventional restitution coefficient between the contact surfaces. It is depends on the characteristics of the contact model.

The virtual mass is basically derived from the link configuration and link inertia property. In addition, the viscosity and stiffness of joints or structures affect the virtual mass value. Mechanical systems have energy dissipation or damping effect, while contact surfaces also have energy dissipation at the time of contact. However, their effect have not been clarified yet. The damping effect complicates the virtual mass model, and it becomes difficult to solve the model because describing energy dissipation by using mass characteristics is difficult.

This section discusses an extension of the virtual mass including the viscosity and stiffness when the impedance system is contacted. A novel virtual mass is redefined as the "virtual mass of impedance system (VMI)" with the approximated contact model. Although the damping term is present in the impedance system, the virtual mass model can be calculated with an assumption of small damping effect. The concept of the VMI model is shown in Fig.7.

A. Definition of Virtual Mass

The equivalent mass m_v of the hand with an impedance is given by the following three approaches.

1) Impulse-Based Virtual Mass: The mechanical impedance system can be approximated as a single virtual mass using the impulse-momentum equation:

$$\int_{t_0}^{t} F dt = m_v \dot{x}_h, \quad (12)$$

where m_v is the virtual mass of impedance. Hence, the virtual mass of impedance is defined as follows:

$$m_v(t) = \frac{\int_{t_0}^{t} F dt}{\dot{x}_h}. \quad (13)$$

Since the virtual mass defined in Eq.(13) changes with time, the average of the virtual mass over a contact duration is used as follows:

$$m_v = \frac{1}{T}\int_{t_0}^{t_e} \frac{\int_{t_0}^{t} F dt}{\dot{x}_h} dt, \quad (14)$$

where $T = t_e - t_0$ is the contact duration of one collision.

2) Energy-based Virtual Mass: In a similar manner, another definition of the virtual mass of impedance is obtained by using the law of conservation of energy as follows:

$$\int_{t_0}^{t} \dot{x}_h F dt = \frac{1}{2} m_v \dot{x}_h^2. \quad (15)$$

Hence, the energy-based m_v at time t is defined as follow:

$$m_v = \frac{2}{\dot{x}_h^2}\int_{t_0}^{t} \dot{x}_h F dt. \quad (16)$$

The time average of the m_v is obtained as follows:

$$m_v = \frac{2}{T}\int_{t_0}^{t_e} \frac{\int_{t_0}^{t_e} \dot{x}_h F dt}{\dot{x}_h^2} dt. \quad (17)$$

B. Formulation of Virtual Mass

1) Contact Force: The theoretical representation of Eqs. (14) and (17) requires hand velocity and contact force. They can be obtained by solving the differential equation Eq.(7). However, in general, a recursive numerical calculation is required in order to solve it because the analytic solution is complicated. In this section, an approximate analytic method is mentioned.

Figure 8 depicts a typical time profile of the contact force of the impedance system. If the damping effects of the impedance system and contact surface are not large, the upward profile from zero to the peak can be approximated by a sinusoidal wave having a frequency of $\omega = 2\pi/T$.

The equation of motion of the impedance system with the sinusoidal force approximation is as follows:

$$\sin(\omega t) = m_i \ddot{x}_h + d_i \dot{x}_h + k_i x_h. \quad (18)$$

Assume that in the frequency domain, the input to the system is the contact force $F(s)$, and the output is the hand acceleration $\ddot{X}(s)$ connected to the following transfer function $G(s)$.

$$\ddot{X}(s) = G(s)F(s). \quad (19)$$

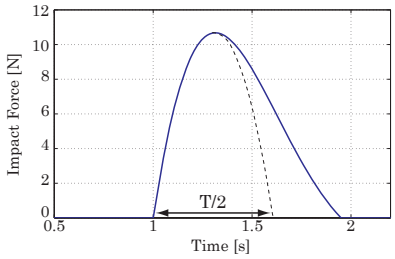

Fig. 8. Typical time profile of the impact force

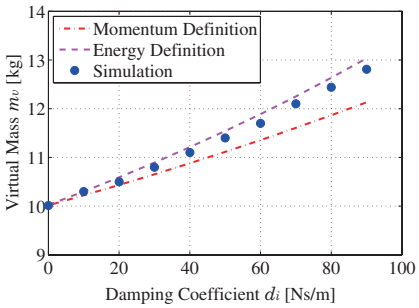

Fig. 9. Virtual mass of impedance system m_v vs. damping coefficient d_i ($m_i = 10$ [kg], $k_i = 50$ [N], $k_c = 5,000$ [N], $d_c = 0$ [Ns/m])

Taking the Laplace transform of Eq.(18) yields the following:

$$\ddot{X}_h(s) = \left(m_i + \frac{d_i}{s} + \frac{k_i}{s^2}\right)^{-1} \frac{\omega}{s^2+\omega^2}. \tag{20}$$

The inverse Laplace transform yields the hand acceleration in the time domain:

$$\ddot{x}_h(t) = |G(j\omega)|^2 \left(\frac{\lambda_1}{\lambda_2}\sin(\lambda_2 t) - \frac{d_i}{\omega}\cos(\lambda_2 t)\right) \cdot \exp\left(-\frac{d_i}{2m_i}t\right) + |G(j\omega)|\sin\Big(\omega t + \angle\big(G(j\omega)\big)\Big) \tag{21}$$

where j is the imaginary number, ω is the natural frequency, and λ_1 and λ_2 are given as follows:

$$\left.\begin{aligned} \lambda_1 &= \frac{1}{m}\left(\frac{k_i^2}{\omega^3} + \frac{d_i^2 - 2m_i k_i}{2\omega}\right) \\ \lambda_2 &= \frac{1}{2m_i}\sqrt{4k_i m_i - d_i^2} \end{aligned}\right\}. \tag{22}$$

Thus, the integration of Eq.(21) yields the hand velocity in the time domain.

$$\dot{x} = \left\{\frac{|G(j\omega)|^2}{\omega}\exp\left(-\frac{d_i}{2m_i}t\right)\right\} \cdot \left\{\left(m_i - \frac{k_i}{\omega^2}\right)\cos(\lambda_2 t) - \frac{d_i}{2m_i\lambda 2}\left(m_i + \frac{k_i}{\omega^2}\right)\sin(\lambda_2 t)\right\} - \frac{|G(j\omega)|}{\omega}\cos\Big(\omega t + \angle\big(G(j\omega)\big)\Big). \tag{23}$$

The natural frequencies ω of the system are approximated as those with no damping.

$$\omega = \left\{\frac{1}{2}\left[\omega_1^2 + \omega_2^2(1+\mu)\right] \pm \frac{1}{2}\sqrt{\left[\omega_1^2 + \omega_2^2(1+\mu)\right]^2 - 4\omega_1^2\omega_2^2}\right\}^{\frac{1}{2}}, \tag{24}$$

where

$$\omega_1 = \sqrt{\frac{k_i}{m_i}}, \quad \omega_2 = \sqrt{\frac{k_c}{m_t}}, \quad \mu = \frac{m_t}{m_i}. \tag{25}$$

When the contact stiffness is considerably larger than the stiffness of the chaser impedance, the force frequency can be approximated to that of the free-end single vibration model. The frequency is obtained as follows:

$$\omega' = \sqrt{\frac{k_c}{\tilde{m}}}, \tag{26}$$

where

$$\tilde{m} = \frac{m_i m_t}{m_i + m_t}. \tag{27}$$

V. Verification of VMI Model

In this section, the theoretical prediction and simulation results of the VMI model are compared. The numerical simulation model is identical to the coupled-vibration model described in section III.

For the simulation, the damping coefficient d_i was varied. The main basis for comparison was the manner in which the damping effect changes the virtual mass m_v. In the simulation result, the m_v was obtained by using Eq.(11).

Two cases of the contact stiffness were examined. The two stiffness values of the contact surface used for the comparison were $k_c = 5,000$ [N/m] and $k_c = 50,000$ [N/m]. The other parameters m_i, k_i, k_c, and d_c remained constant.

The mass m_i and stiffness k_i of the impedance system were 10 [kg] and 50 [N/m], respectively. The damping coefficient of the contact surface was assumed as $d_c = 0$ [Ns/m], and the target mass m_t was 50 [kg]. The impedance system was initially unstretched and is in its equilibrium state.

Figures 9 and 10 show the virtual mass m_v obtained by the dynamics simulation result and the predicted m_v based on the momentum definition and energy definition.

The results represent that both predictions by Eqs. (14) and (17) are close to the simulation results. However, when the damping effect is larger, the deviation between them are larger because the waveform of the contact force become different from the sinusoidal. Therefore, when m_v is predicted by using the proposed method in practice, a margin of error should be considered.

VI. Condition of Maintaining the Contact with the Target

At the moment of contact, the contact force fatally gives the target velocity. The required condition for maintaining or repeating contact with the target after the initial contact can be formulated as follows:

$$\mathrm{sgn}(\dot{\boldsymbol{x}}'_{\mathrm{h}} - \dot{\boldsymbol{x}}'_{\mathrm{t}}) > 0 \tag{28}$$

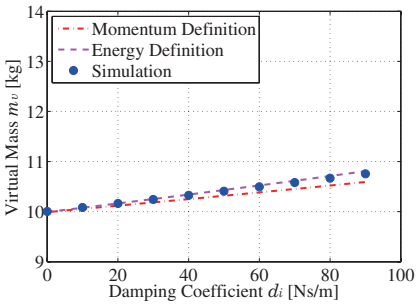

Fig. 10. Virtual mass of impedance system m_v vs. damping coefficient d_i ($m_i = 10$ [kg], $k_i = 50$ [N], $k_c = 50,000$ [N], $d_c = 0$ [Ns/m])

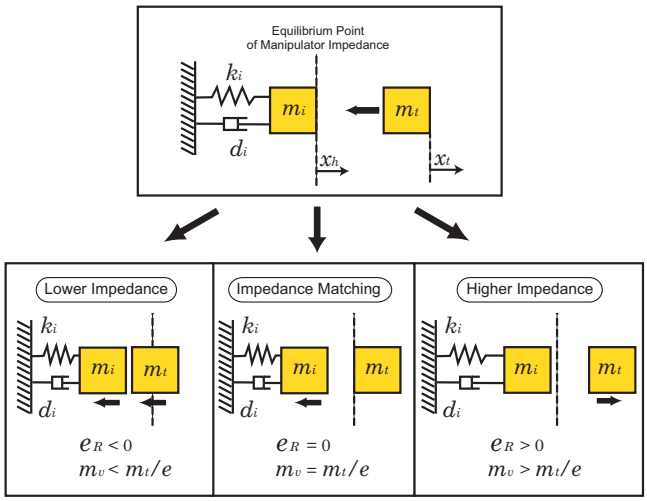

Fig. 11. Post-contact behavior of target

or

$$|\dot{\boldsymbol{x}}'_h| \geq |\dot{\boldsymbol{x}}'_t| \quad \text{and} \quad \mathrm{sgn}(\dot{\boldsymbol{x}}'_\mathrm{h}) \cdot \mathrm{sgn}(\dot{\boldsymbol{x}}'_\mathrm{t}) = 1, \qquad (29)$$

where $\dot{\boldsymbol{x}}'_h$ and $\dot{\boldsymbol{x}}'_t$ are the post-contact velocities of the chaser hand and target, respectively. Equation (28) represents the condition when the relative velocity is negative. Equation (29) represents condition that the direction is same as that of the target velocity, and the hand velocity is greater than the target velocity. The velocity of the hand and target after the contact should be controlled such that the above conditions are met.

Figure 11 shows the classification of the relative post-contact behavior of the target based on the manipulator impedance. In order to satisfy the conditions for maintaining the contact (Eqs. (28) and (29)), $-1 < e_R \leq 0$ should be satisfied. the When the $e_R = 0$, the target stops at the equilibrium point of the impedance just after the contact. In this case, the entire kinetic energy of the target is transferred to the manipulator. According to Eq. (11), this phenomenon occurs when $m_v = m_t/e$ (when $e \neq 0$). This condition is so-called "impedance matching." On the basis of the VMI model, the post-contact velocity is given by Eq.(11). When the manipulator impedance is less than the impedance matching condition, that is $m_v < m_t/e$, the target pushes the manipulator inside the equilibrium point ($-1 < e_R < 0$). In this case, the target repeats the contacts and the kinetic energy is gradually transferred to the impedance system. On the other hand, when impedance is higher, the target bounces off the manipulator immediately after the contact ($e_R > 0$), which implies that the capture is failed. Therefore, the impedance characteristics should be set so that m_v is lower than m_t/e including the margin of the calculation error.

VII. Conclusion

In this paper, the relationship between the post-contact motion of the target and contact parameters has been clarified. The VMI model was defined as an evaluation index of the target's post-contact motion. This model projected the impedance characteristics to a mass property. The virtual mass gives the post-contact motion of the target. The accuracy of the virtual mass model was verified by comparing predicted and simulated values. By using these criteria, the conditions for maintaining the contact were clarified. The boundary condition to maintain the contact is given as VMI matching the target inertia. When the hand impedance is lower than the boundary condition, the robot hand can maintain contact with the target.

VIII. Acknowledgments

This research was partially supported by the Ministry of Education, Science, Sports and Culture, Grant-in-Aid for Young Scientists (B), 2009, No. 20760155.

References

[1] T. Kasai, M. Oda, and T. Suzuki, "Results of the ETS-7 Mission - Rendezvous Docking and Space Robotics Experiments," Proc. 5th Int. Symp. on AI, Robotics and Automation in Space, iSAIRAS'99, pp.299-306, 1999.

[2] Shoemaker, J, Wright, M, "Orbital express on-orbit satellite servicing demonstration," Proc. of the SPIE Defense and Security Symposium 2004, Vol. 5419-09, Orlando, Florida, April 2004

[3] K.Yoshida et al., "Dynamics, Control, and Impedance Matching for Robotic Capture of a Non-cooperative Satellite," RSJ Advanced Robotics, Vol.18, No.2, pp.175-198, 2004.

[4] S. Ali A. Moosavian, R. Rastegari, E. Papadopoulos, "Multiple Impedance Control for Space Free-Flying Robots," AIAA Journal of Guidance, Control, and Dynamics, Vol. 28, No. 5, pp.939-947, 2005.

[5] Pushparaj Mani Pathak, Amalendu Mukherjee and Anirvan Dasgupta, "Impedance control of space robot," Proc. of 15th IASTED International Conference MODELING AND SIMULATION, pp.356-361,2004

[6] Haruhiko Asada, "A geometrical representation of manipulator dynamics and its application to arm design", Journal of Dynamic Systems, Measurement, and Control, Vol.105, No.3, pp.131-135, 1983.

[7] K.Yoshida, R.Kurazume, N.Sashida and Y.Umetani, "Modeling of collision dynamics for space free-floating links with extended generalized inertia tensor," in Proc. IEEE Int. Conf. on Robotics and Automation, Nice, pp.899-904, 1992

[8] G. Gilardi, I. Sharf, "Literature survey of contact dynamics modeling," Mechanism and Machine Theory, 37 pp.1213-1239, 2002.

[9] Hiroki Nakanishi and Kazuya Yoshida, "Impedance Control for Free-flying Space Robots -Basic Equations and Applications-," Proc. of IEEE/RSJ International Conf. on Intelligent Robots and Systems, pp.3137-3142, 2006

[10] Y.Umetani and K.Yoshida, "Resolved Motion Rate Control of Space Manipulators with Generalized Jacobian Matrix," IEEE Trans. on Robotics and Automation, 5, 3, pp.303-314 1989.